Supplementary Material

Monolayer SnS_2 Schottky Barrier Field Effect Transistors: Effect of Electrodes

Hong Li[1,*], Yunfeng Zhang[1], Fengbin Liu[1], and Jing Lu[2, 3, 4*]

[1] College of Mechanical and Material Engineering, North China University of Technology, Beijing 100144, P. R. China

[2] State Key Laboratory of Mesoscopic Physics and Department of Physics, Peking University, Beijing 100871, P. R. China

[3] Collaborative Innovation Center of Quantum Matter, Beijing 100871, P. R. China

[4] Peking University Yangtze Delta Institute of Optoelectronics, Nantong 226000, P. R. China

*Corresponding author: jinglu@pku.edu.cn; lihong@ncut.edu.cn

Table S1. Energy differences between each stacking pattern and the most stable stacking pattern of the 1T-$NbTe_2/SnS_2$ and 2H-$NbTe_2/SnS_2$ vdW heterostructures. d_v is the vertical distance between the two layers. $\Phi_n^{\perp}$ is the *n*-type vertical Schottky barrier.

		Atop-I	Atop-II	Fcc-I	Fcc-II	Hcp-I	Hcp-II
1T-$NbTe_2/SnS_2$	$\triangle E$ (eV)	0.22	0.226	0.034	0	0.052	0.05
	d_v (Å)	3.5715	3.6042	2.8547	2.6873	2.9039	2.9452
	$\Phi_n^{\perp}$(eV)	0.051	-0.047	0.093	0.105	-0.084	-0.019
2H-$NbTe_2/SnS_2$	$\triangle E$ (eV)	0.221	0.229	0.025	0	0.054	0.033
	d_v (Å)	3.5991	3.6504	2.8622	2.7181	2.93	2.9186
	$\Phi_n^{\perp}$(eV)	0.036	0	0.4	0.385	-0.012	0.223

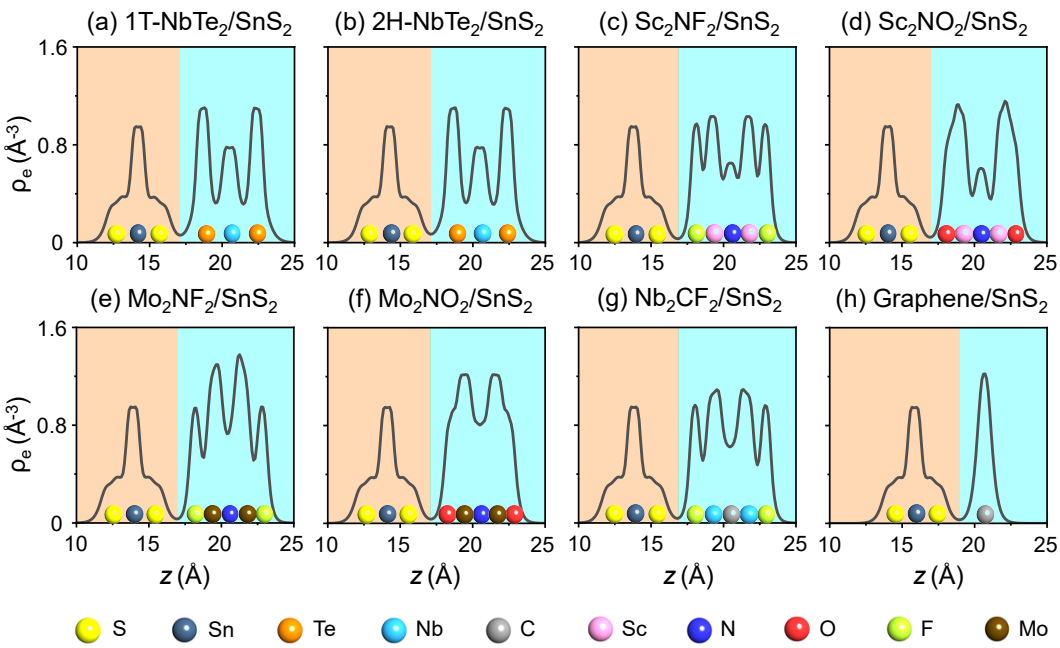

Figure S1. The plane-averaged electron densities of the (a) 1T-$NbTe_2/SnS_2$, (b) 2H-$NbTe_2/SnS_2$, (c) Sc_2NF_2/SnS_2, (d) Sc_2NO_2/SnS_2, (e) Mo_2NF_2/SnS_2, (f) Mo_2NO_2/SnS_2, (g) Nb_2CF_2/SnS_2, and (h) graphene/SnS_2 vdW heterostructures.

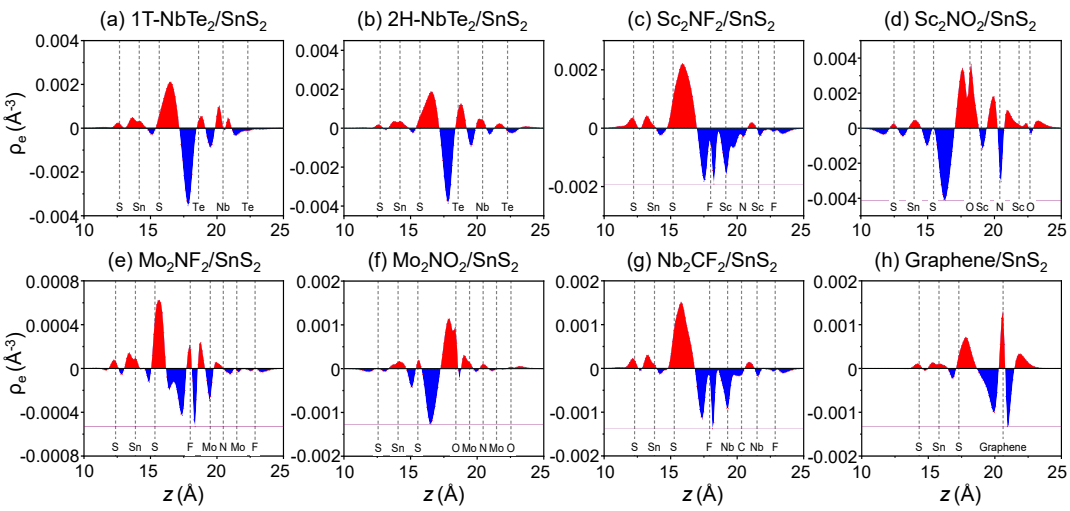

Figure S2. The plane-averaged electron density differences of the (a) 1T-$NbTe_2/SnS_2$, (b) 2H-$NbTe_2/SnS_2$, (c) Sc_2NF_2/SnS_2, (d) Sc_2NO_2/SnS_2, (e) Mo_2NF_2/SnS_2, (f) Mo_2NO_2/SnS_2, (g) Nb_2CF_2/SnS_2, and (h) graphene/SnS_2 vdW heterostructures.

Figure S3. The vertical Schottky barrier ($\Phi_n^{\perp}/\Phi_p^{\perp}$) between ML SnS_2 and various ML metals. The diagonal line denotes the values predicted by the Schottky-Mott model.

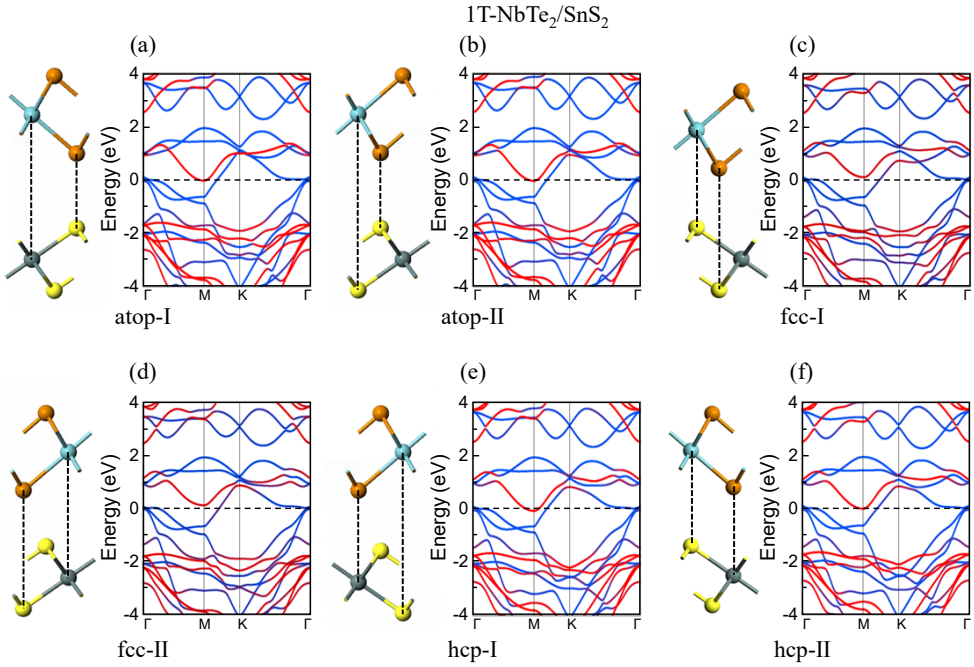

Figure S4. The stacking patterns and projected band structures of the 1T-$NbTe_2/SnS_2$ vdW heterostructure. (a) Atop-I. (b) Atop-II. (c) Fcc-I. (d) Fcc-II. (e) Hcp-I. (f) Hcp-II.

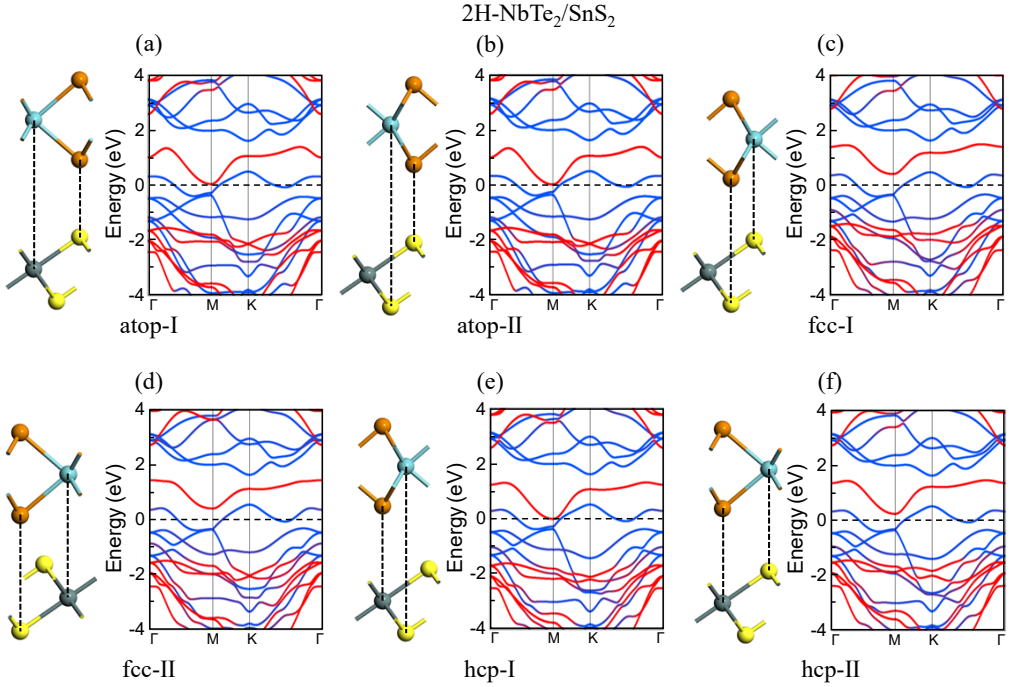

Figure S5. The stacking patterns and projected band structures of the 2H-$NbTe_2/SnS_2$ vdW heterostructure. (a) Atop-I. (b) Atop-II. (c) Fcc-I. (d) Fcc-II. (e) Hcp-I. (f) Hcp-II.

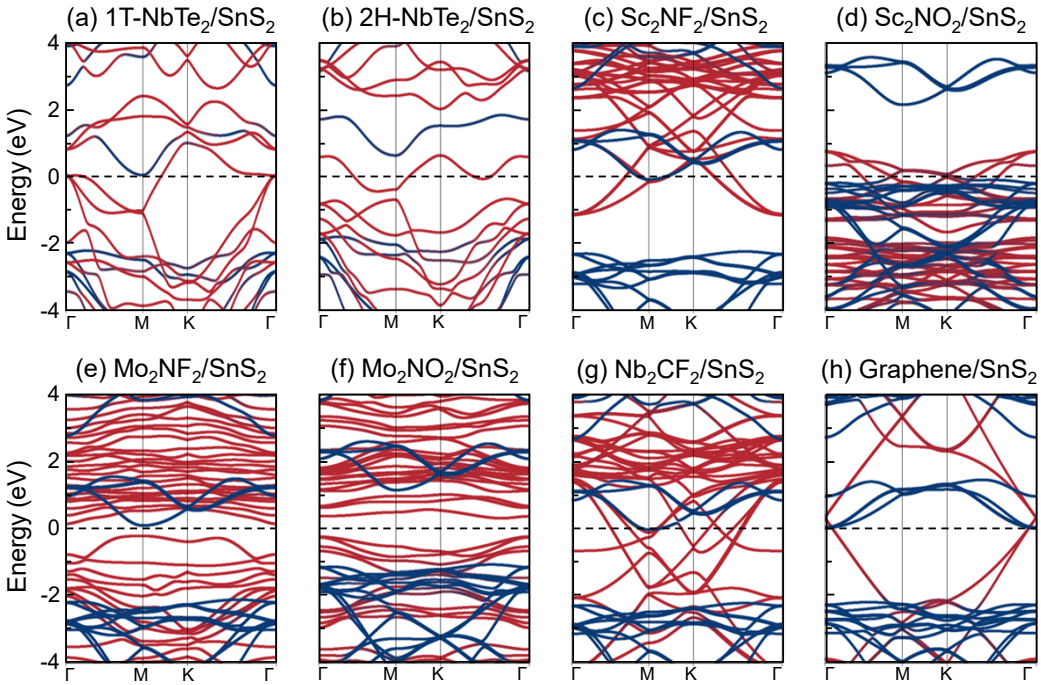

Figure S6. Projected band structures with HSE functional of the (a) 1T-$NbTe_2/SnS_2$, (b) 2H-$NbTe_2/SnS_2$, (c) Sc_2NF_2/SnS_2, (d) Sc_2NO_2/SnS_2, (e) Mo_2NF_2/SnS_2, (f) Mo_2NO_2/SnS_2, (g) Nb_2CF_2/SnS_2, and (h) graphene/SnS_2 vdW heterostructures.

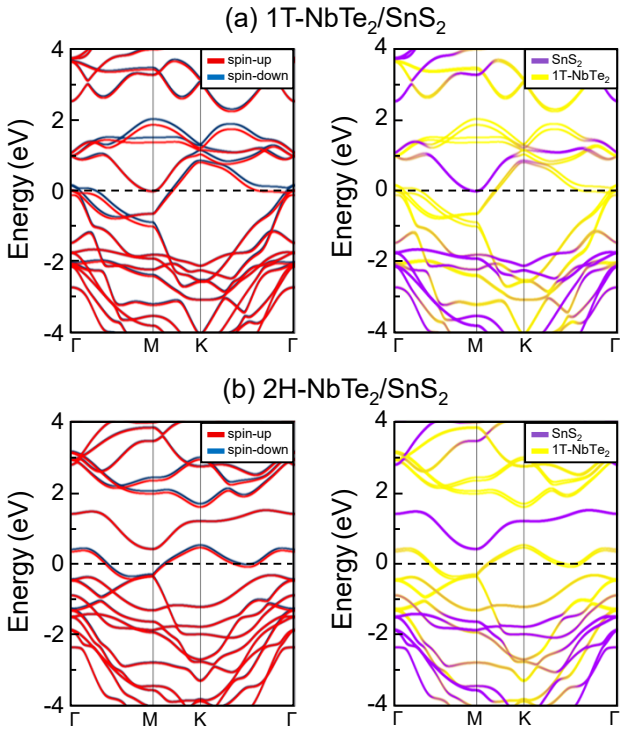

Figure S7. Spin-polarized projected band structures of the (a) 1T-$NbTe_2/SnS_2$ and (b) 2H-$NbTe_2/SnS_2$ vdW heterostructures. Left panel: projected on spins. Right panel: projected on layers.